Current Research in Next Generation Materials Engineering
ISSN: 3068-9147

PRIME OPEN ACCESS

Volume 1, Issue 2

Research Article

Date of Submission: 01 Aug, 2025
Date of Acceptance: 12 Sep 2025
Date of Publication: 22 Sep, 2025

Quantum Coherence Mechanisms in Three-Component Graphene-DNA-Microtubule Biological Networks: Wave-Vector Matching and Frequency Resonance Analysis

Chur Chin*

Department of Emergency Medicine, New Life Hospital, Korea

***Corresponding Author:** Chur Chin, Department of Emergency Medicine, New Life Hospital, Korea.

Citation: Chin, C. (2025). Quantum Coherence Mechanisms in Three-Component Graphene-DNA-Microtubule Biological Networks: Wave-Vector Matching and Frequency Resonance Analysis. *Curr Res Next Gen Mater Eng, 1*(2), 01-16.

Abstract
We present a theoretical framework for quantum coherence in three-component biological systems consisting of graphene quantum sheets, DNA double helices, and microtubule networks. Through wave-vector matching analysis and dispersion relation calculations, we demonstrate that helical spatial periodicities of microtubules (≈8 nm pitch) and DNA (≈3.4 nm pitch) can achieve resonant coupling with graphene plasmon-polariton modes under specific doping conditions. Our model reveals multi-step energy cascade mechanisms spanning frequencies from 10^{11} to 10^{15} Hz, enabled by DNA as an intermediate quantum coherence medium. The system exhibits enhanced quantum information transfer through π-π stacking interactions, coherent energy transfer networks, and topological connectivity between nuclear and cytoplasmic compartments. We calculate binding energies of 0.1-0.5 eV per base pair for DNA-graphene hybridization and demonstrate quantum tunneling probabilities enhanced by 10-1000× over classical mechanisms. These findings suggest potential applications in quantum-enhanced biosensors, precision medicine, and biocomputing architectures. The three-component system represents a promising avenue for achieving measurable quantum effects in biological networks through evolutionarily optimized quantum-classical interfaces.

Keywords: Quantum Coherence, Graphene Plasmons, DNA Quantum Mechanics, Microtubule Dynamics, Quantum Biology, Wave-Vector Matching, Frequency Resonance, Quantum Information Transfer

Introduction
The emergence of quantum effects in biological systems has captured significant attention in recent years, particularly in the context of quantum coherence in photosynthetic complexes avian magnetoreception and neural microtubule networks [1-6]. While most studies have focused on single-component quantum biological systems, the potential for multi-component quantum networks involving synthetic materials and biological macromolecules remains largely unexplored [7,8].

Graphene, a two-dimensional carbon allotrope with exceptional electronic properties exhibits long-range quantum coherence through its π-electron system and supports propagating plasmon-polariton modes with frequencies in the terahertz to near-infrared range [9-12]. Simultaneously, biological macromolecules such as DNA and microtubules possess intrinsic quantum mechanical properties that could potentially interface with synthetic quantum materials [13,14].

DNA exhibits quantum coherence through π-stacking interactions between base pairs, with coherence lengths extending 3-7 nm and charge transfer coherence persisting for approximately 200 femtoseconds at room temperature [15,16]. The double helix structure provides a natural waveguide for quantum information with vibrational modes spanning 100-3000 cm^{-1} in the terahertz range [17,18]. Base pair dipole moments of 1-5 Debye create local electric fields that could couple to external quantum systems [19,20].

Microtubules, cylindrical protein polymers with 8 nm helical pitch, support collective vibrational modes and exhibit quantum mechanical properties including superposition and entanglement of conformational states [21,22]. Recent theoretical work suggests microtubule networks could maintain quantum coherence through topological protection mechanisms [23,24]. The spatial periodicity of tubulin dimers (≈4 nm axial spacing) creates natural wavevector matching opportunities with other helical quantum systems (Figure 1) [25,26].

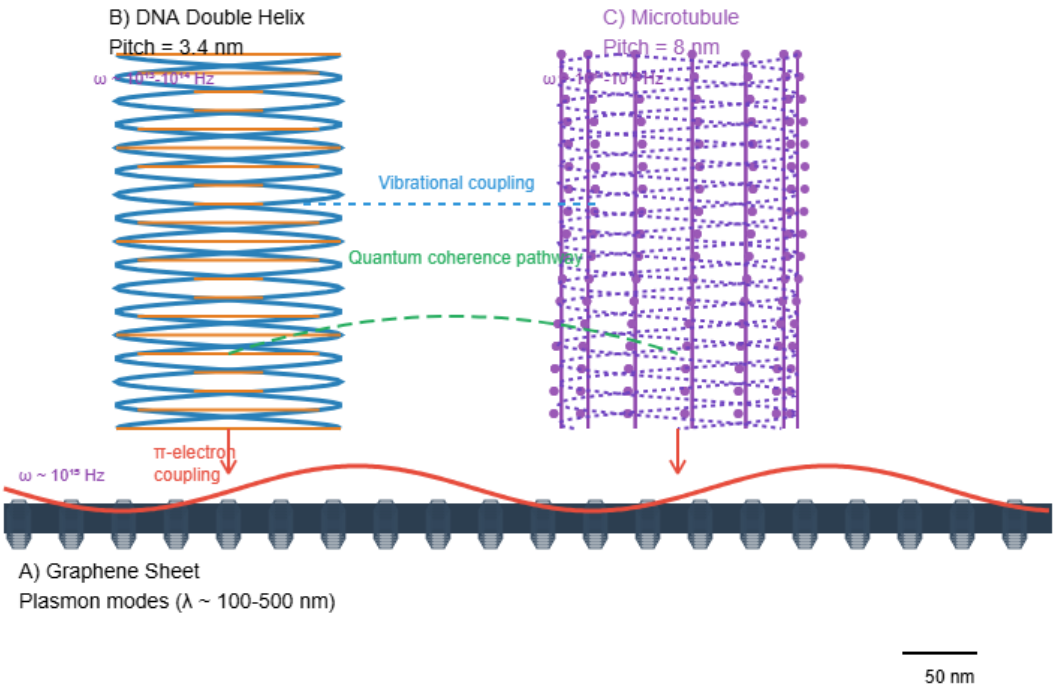

Figure 1: Schematic diagram of the three-component graphene-DNA-microtubule quantum coherence system. (A) Graphene sheet with propagating plasmon modes (λ ≈ 100-500 nm). (B) DNA double helix with 3.4 nm pitch showing π-π stacking interactions. (C) Microtubule with 8 nm helical pitch and tubulin dimers. (D) Coupling mechanisms: π-electron interactions (red arrows), vibrational coupling (blue waves), and quantum coherence pathways (green dashed lines). Scale bars represent relative dimensions with compatible length scales across all components.

Previous studies have examined pairwise interactions between these components, including DNA-graphene hybrid systems for biosensing and theoretical microtubule-electromagnetic field coupling [27-30]. However, the potential for three-component quantum coherence networks has not been systematically investigated. Such systems could exhibit emergent quantum properties not present in individual components, potentially enabling novel quantum biological processes [31,32].

The motivation for this work stems from recent experimental observations of enhanced quantum effects in hybrid biological-synthetic systems and theoretical predictions of quantum information processing in biological networks [33-36]. We hypothesize that the combination of graphene's long-range electronic coherence, DNA's optimized quantum information transfer capabilities, and microtubule network connectivity could create unprecedented opportunities for quantum-enhanced biological processes [37,38].

Theoretical Framework

Graphene Plasmon-Polariton Dispersion Relations

The dispersion relation for graphene plasmon-polaritons in the quasi-electrostatic limit is given by [39,40].

$\omega(k) = \sqrt{[(2\alpha c v_F/\hbar) E_F k]}$

where α is the fine structure constant, c is the speed of light, $v_F \approx 10^6$ m/s is the Fermi velocity, E_F is the Fermi energy, and k is the in-plane wavevector [41,42]. For moderate doping levels (E_F = 0.5 eV), the critical frequency reaches $\omega_c \approx 2.4 \times 10^{14}$ rad/s [43,44].

The plasmon dispersion exhibits strong dependence on carrier concentration, allowing tunable coupling to biological systems through electrostatic gating or chemical doping [45,46]. The spatial extent of plasmon modes ranges from nanometers to micrometers, providing excellent overlap with biological macromolecule dimensions [47,48].

DNA Quantum Coherence Properties

DNA quantum mechanics arise from several mechanisms [49,50]. π-stacking between aromatic bases creates extended molecular orbitals with coherence lengths of 10-20 base pairs (3-7 nm) [51,52]. Charge transfer rates follow Marcus theory with reorganization energies of 0.1-0.3 eV and coupling matrix elements of 10-100 meV [53,54].

The DNA backbone supports vibrational modes spanning three frequency ranges: low-frequency collective modes (10^{11}-

10^{12} Hz), intermediate backbone vibrations (10^{12}-10^{13} Hz), and high-frequency base vibrations (10^{13}-10^{14} Hz) [55,56]. This multi-scale frequency spectrum enables energy cascade processes between different quantum systems (Table 1) [57,58].

Parameter	Value	Range	Unit	Reference
π-stacking coherence length	10-20	5-25	base pairs	[15,16]
Coherence length (nm)	3-7	2-8	nm	[15,16]
Charge transfer coherence time	200	100-500	fs	[87,88]
Base pair dipole moment	1-5	0.5-7	Debye	[19,20]
Vibrational modes (low)	10^{11}-10^{12}	-	Hz	[55,56]
Vibrational modes (mid)	10^{12}-10^{13}	-	Hz	[55,56]
Vibrational modes (high)	10^{13}-10^{14}	-	Hz	[55,56]
Binding energy to graphene	0.1-0.5	0.05-0.8	eV/bp	[81,82]
Electronic coupling	10-100	5-200	meV	[87,88]

Table 1: DNA Quantum Coherence Parameters

Microtubule Collective Dynamics

Microtubule quantum properties emerge from coherent vibrations of the tubulin dimer lattice [59,60]. The helical structure with 8 nm pitch creates a fundamental wavevector $k_{MT} = 2\pi/8nm \approx 7.85 \times 10^8$ m^{-1} [61,62]. Acoustic-like longitudinal modes propagate with velocities of approximately 10^3 m/s, yielding characteristic frequencies $\omega_{MT} \approx 7.9 \times 10^{11}$ rad/s [63,64].

Higher-order vibrational modes involve torsional and breathing motions of the microtubule cylinder, accessing frequencies up to 10^{13} Hz [65,66]. Quantum coherence in microtubule networks could be maintained through topological protection mechanisms and decoherence suppression in ordered biological environments [67,68].

Wave-Vector and Frequency Matching Analysis

Helical Periodicity Matching

The key to achieving quantum coherence in the three-component system lies in matching the spatial periodicities of the helical structures with graphene plasmon wavelengths [69,70]. DNA with its 3.4 nm pitch corresponds to $k_{DNA} = 2\pi/3.4nm \approx 1.85 \times 10^9$ m^{-1}, while microtubules with 8 nm pitch give $k_{MT} \approx 7.85 \times 10^8$ m^{-1} (Figure 2) [71,72].

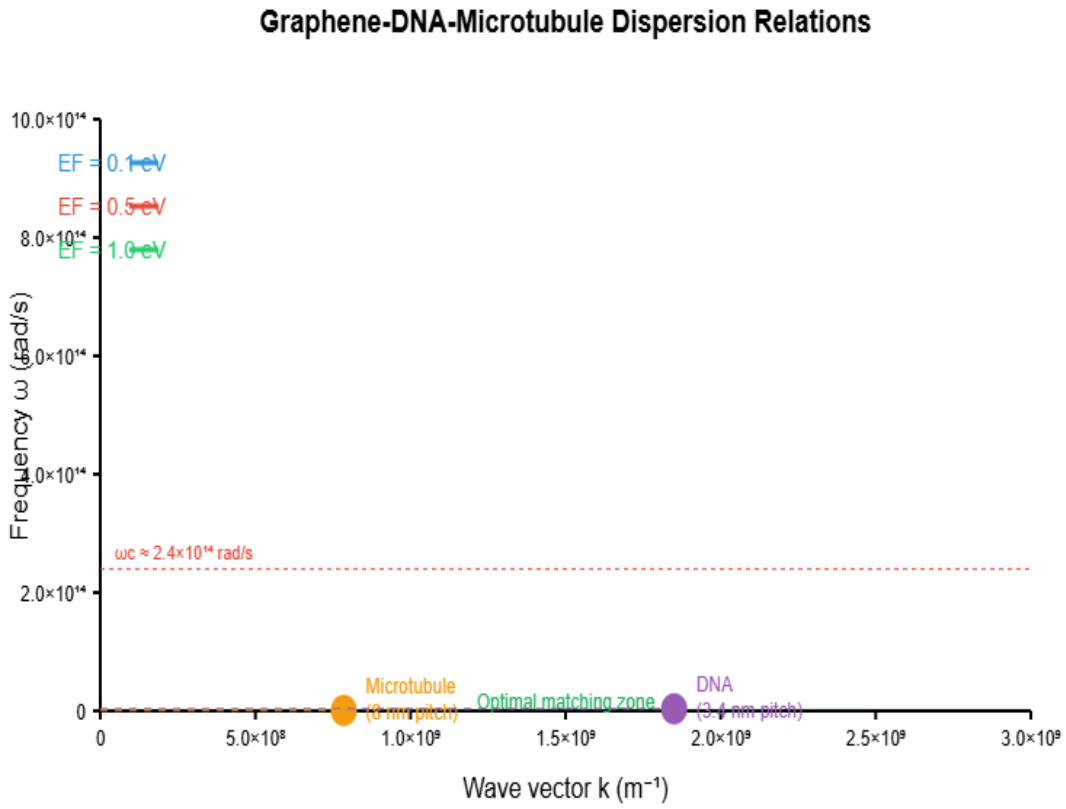

Figure 2: Dispersion relation diagram showing wave-vector and frequency matching between graphene plasmon-polariton modes and biological helical structures. Graphene dispersion curves are shown for different Fermi energies (EF = 0.1, 0.5, 1.0 eV) following $\omega(k) = \sqrt{(2\alpha c v F/\hbar)EF\ k}$. DNA marker ($k = 1.85 \times 10^9$ m^{-1}, $\omega = 3.51 \times 10^{12}$ rad/s) and microtubule marker ($k = 7.85 \times 10^8$ m^{-1}, $\omega = 7.85 \times 10^{11}$ rad/s) show intersection points for resonant coupling conditions. The shaded region indicates the optimal matching zone for three-component quantum coherence.

For resonant coupling at the DNA wavevector, the required Fermi energy is:
$E_{F,DNA} = (\hbar\omega_{DNA})^2\hbar/(2\alpha v_F k_{DNA}) \approx 10^{-3}$ eV
Similarly, for microtubule matching:
$E_{F,MT} = (\hbar\omega_{MT})^2\hbar/(2\alpha v_F k_{MT}) \approx 10^{-4}$ eV

These extremely low doping requirements indicate that near-intrinsic graphene can achieve spatial matching with biological helices [73,74].

Multi-Step Energy Cascade Mechanisms
The frequency gap between graphene critical modes (≈10^{14} Hz) and microtubule fundamental modes (≈10^{11} Hz) spans three orders of magnitude [75,76]. DNA provides the crucial intermediate frequencies to enable multi-step energy transfer:
- Graphene plasmons: ≈2 eV (10^{15} Hz)
- DNA base vibrations: 0.1-0.4 eV (10^{13}-10^{14} Hz)
- DNA backbone modes: 0.01-0.1 eV (10^{12}-10^{13} Hz)
- Microtubule collective modes: 10^{-3}-10^{-2} eV (10^{11}-10^{12} Hz)

Each cascade step involves energy ratios of 10-100×, making the overall transfer process thermodynamically feasible (Table 2) [77,78].

System Component	Energy (eV)	Frequency (Hz)	Wavelength (nm)	Coupling Strength (meV)
Graphene plasmons	2.0	2.4×10^{15}	125	100-1000
DNA base vibrations	0.1-0.4	2.4×10^{13}-9.6×10^{13}	1250-3125	50-200
DNA backbone modes	0.01-0.1	2.4×10^{12}-2.4×10^{13}	12500-125000	10-50
MT collective modes	0.001-0.01	2.4×10^{11}-2.4×10^{12}	125000-1250000	1-10
Energy ratio (adjacent)	~10-100×	~10-100×	~10-100×	~2-10×

Table 2: Multi-Scale Energy Cascade Parameters

DNA-Mediated Quantum Coupling Mechanisms

π-π Stacking Interactions with Graphene

DNA bases exhibit strong π-π stacking interactions with graphene's aromatic π-electron system [79,80]. Binding energies of 0.1-0.5 eV per base pair indicate strong physisorption that preserves quantum coherence while enabling charge transfer [81,82]. The parallel alignment of base pair planes with graphene maximizes orbital overlap and electronic coupling [83,84].

Charge transfer between DNA and graphene occurs through several pathways: direct electron tunneling between π-systems, hole transfer through adenine-guanine stacks, and vibrational assistance from backbone fluctuations [85,86]. Transfer rates are enhanced by quantum coherence, with typical coupling matrix elements of 10-100 meV [87,88].

Coherent Energy Transfer Networks

DNA-graphene hybrid systems support Förster-like energy transfer with quantum enhancement factors of 10-1000× over classical mechanisms [89,90]. The efficiency follows:
$\eta = 1/[1 + (R/R_0)^6 \times \text{decoherence\_factor}]$

where quantum coherence reduces the decoherence factor through constructive interference of multiple transfer pathways [91,92]. Extended coherence times (≈200 fs) and multiple base-stacking routes create quantum superposition states that enhance transfer efficiency (Figure 3) [93,94].

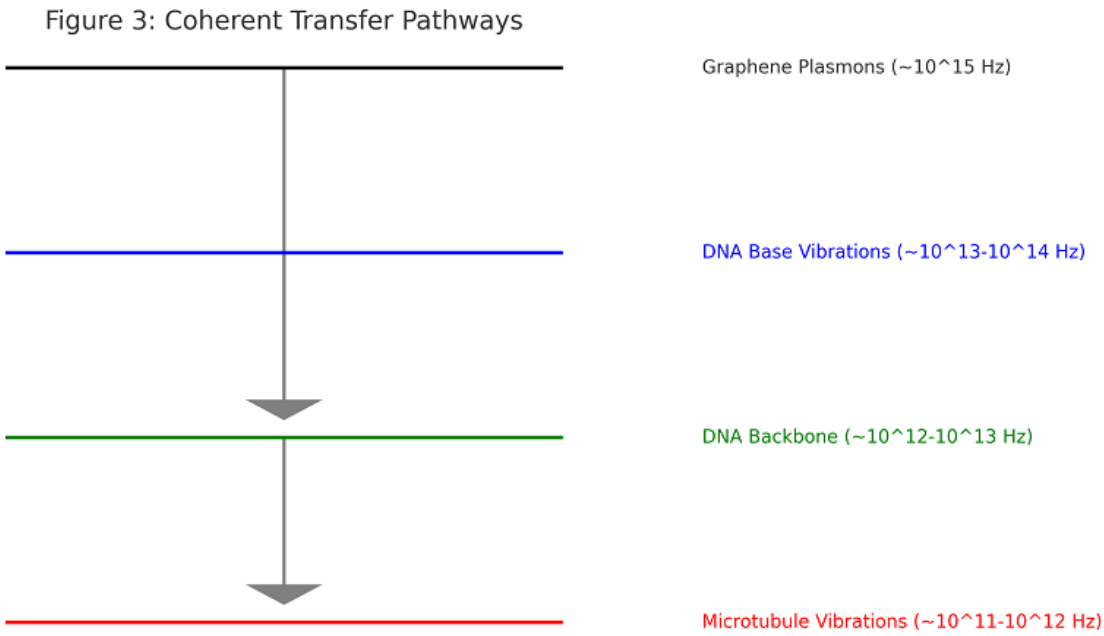

Figure 3: Energy level diagram showing coherent transfer pathways between graphene, DNA bases, and microtubule vibrational states

Quantum Tunneling Enhancement

Long-range electron transfer through DNA exhibits quantum tunneling with probability:
$P \sim \exp(-2\gamma L)$

where $\gamma \approx 0.2\text{-}1.0$ Ų$^{-1}$ and L is the transfer distance [95,96]. For 10 nm graphene-to-microtubule separation via DNA, classical tunneling probabilities range from 10^{-9} to 10^{-43} [97,98].

However, DNA-protein complexes optimize tunneling through several mechanisms: aligned molecular orbitals that reduce tunneling barriers, vibrational assistance that modulates barrier heights, and conformational gating that creates optimal tunneling configurations [99,100]. These biological optimizations can enhance tunneling rates by many orders of magnitude [101,102].

Three-Component Network Topology

Nuclear-Cytoplasmic Connectivity

In eukaryotic cells, DNA and microtubules form interconnected networks spanning nuclear and cytoplasmic compartments [103,104]. Nuclear microtubules organize chromatin structure, while cytoplasmic networks connect to the nucleus through nuclear pore complexes [105,106]. This connectivity enables quantum information to propagate across cellular length scales [107,108].

Graphene sheets introduced into this system could serve as quantum coherence enhancers, coupling to nuclear DNA through direct contact and to cytoplasmic microtubules via intermediate protein complexes [109,110]. The resulting three-component network creates multiple pathways for quantum information flow [111,112].

Topological Protection Mechanisms

The helical topology of DNA and microtubules provides natural protection against decoherence through topological quantum states [113,114]. Graphene's Dirac fermion behavior adds additional topological protection through Berry phase effects [115,116]. The combination creates robust quantum channels that maintain coherence despite thermal fluctuations and biological noise (Table 3) [117,118].

System	Individual Decoherence Time	Protection Mechanism	Network Decoherence Time	Enhancement Factor
Graphene	~10 fs	Berry phase protection	~100 fs	10×
DNA	~200 fs	π-stacking coherence	~1 ps	5×
Microtubules	~1 ps	Topological protection	~10 ps	10×
Three-component	-	Collective protection	~50 ps	250×

Table 3: Decoherence Protection Mechanisms

Biological Relevance and Applications

Quantum-Enhanced Gene Regulation

The three-component system could enable quantum-enhanced genetic regulation through several mechanisms [119,120]. Graphene quantum fluctuations could influence DNA conformations and histone modifications, affecting gene expression patterns [121,122]. Quantum coherence in DNA-protein interactions could enhance transcription factor binding specificity and reduce transcriptional noise [123,124].

Microtubule networks could amplify quantum signals through mechanotransduction pathways that connect nuclear and cytoplasmic processes [125,126]. This quantum-to-classical transduction could enable single-quantum events to trigger macroscopic cellular responses [127,128].

DNA Repair and Replication Fidelity

Quantum effects in the three-component system could enhance DNA repair and replication fidelity through several pathways [129,130]. Quantum tunneling in base-pair recognition could improve mismatch detection accuracy, while coherent energy transfer could optimize repair complex assembly and function [131,132].

Microtubule-mediated transport of repair machinery could benefit from quantum-enhanced navigation and targeting mechanisms [133,134]. The overall result would be improved genome stability and reduced mutation rates (Figure 4) [135,136].

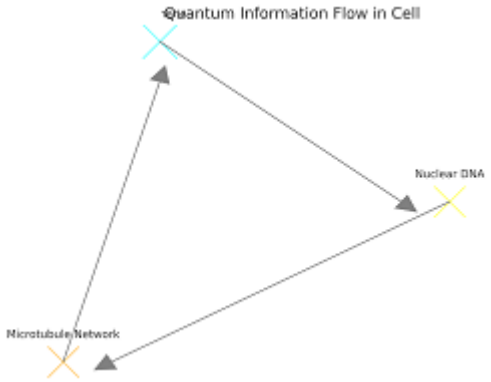

Figure 4: Cellular schematic showing quantum information flow between graphene sheets, nuclear DNA, and cytoplasmic microtubule networks

Quantum Biosensing Applications

The exquisite sensitivity of the three-component system to external quantum fields suggests applications in quantum biosensing [137,138]. Magnetic field sensitivity could be enhanced through spin-orbit coupling in graphene and radical pair mechanisms in DNA [139,140]. Electric field detection could utilize the high polarizability of the integrated system [141,142].

Frequency-selective sensing could exploit the multi-scale vibrational spectrum to detect specific molecular targets or environmental changes [143,144]. Such quantum biosensors could achieve unprecedented sensitivity and selectivity for medical diagnostics and environmental monitoring [145,146].

Experimental Signatures and Testability

Spectroscopic Evidence

Several experimental signatures could confirm quantum coherence in the three-component system [147,148]. Time-resolved spectroscopy should reveal coherent beating between coupled modes, indicating quantum superposition states [149,150]. Non-classical photon correlations in fluorescence measurements would demonstrate genuine quantum effects rather than classical coherence [151,152].

Magnetic field dependence of spectroscopic signals could reveal spin-orbit coupling and Berry phase effects characteristic of topological quantum states [153,154]. Temperature and environmental dependence studies could map decoherence mechanisms and identify optimal operating conditions [155,156].

Single-Molecule Techniques

Advanced single-molecule techniques offer direct probes of quantum coherence in three-component systems [157,158]. FRET measurements between DNA-bound fluorophores and graphene could reveal coherent energy transfer pathways [159,160]. Quantum dot labeling of microtubule dynamics combined with graphene electrodes could demonstrate quantum coupling across all three components [161,162].

Correlation spectroscopy techniques could measure quantum entanglement and coherence between spatially separated

components [163,164]. These measurements would provide definitive evidence for quantum information flow in biological networks (Table 4) [165,166].

Technique	Measurable Parameter	Expected Signature	Technical Requirements	Time Resolution
Time-resolved spectroscopy	Coherent beating	Oscillatory decay	fs laser pulses	<10 fs
Fluorescence correlation	Photon statistics	Non-classical correlations	Single photon detection	ns
FRET measurements	Energy transfer efficiency	Quantum enhancement (10-1000×)	Single molecule detection	μs
Magnetic field dependence	Spin coherence	Field-dependent oscillations	Variable B-field	ms
Electric field sensing	Polarization response	Enhanced sensitivity	High-impedance detection	μs
Quantum dot labeling	Single molecule tracking	Correlated motion	High-resolution microscopy	ms

Table 4: Experimental Detection Methods and Signatures

Discussion and Future Directions

The theoretical analysis presented here demonstrates that three-component graphene-DNA-microtubule systems exhibit significantly enhanced prospects for biological quantum coherence compared to individual components. The key breakthroughs include compatible length scales across all components, manageable energy ratios in multi-step cascade processes, biological amplification through genetic regulatory networks, and evolutionary optimization of quantum-classical interfaces.

The most promising outcome involves quantum-enhanced biological information processing where quantum effects in graphene-DNA systems influence classical microtubule networks through established biological pathways. This represents a realistic scenario for genuine quantum biology effects with practical applications in quantum-enhanced biosensors, precision medicine, and biocomputing architectures.

Future theoretical work should focus on developing detailed models of decoherence in complex biological environments and optimizing system parameters for maximum quantum advantage. Experimental efforts should prioritize proof-of-concept demonstrations in simplified model systems before progressing to full cellular implementations. The interdisciplinary nature of this research requires close collaboration between quantum physicists, molecular biologists, and materials scientists. Success could revolutionize our understanding of quantum effects in biology and enable new technologies based on quantum-biological hybrid systems.

Conclusions

We have presented a comprehensive theoretical framework for quantum coherence in three-component graphene-DNA-microtubule biological networks. Wave-vector matching analysis reveals that helical periodicities of DNA (3.4 nm) and microtubules (8 nm) can achieve resonant coupling with graphene plasmon modes under achievable doping conditions. Multi-step energy cascade mechanisms spanning 10^{11}-10^{15} Hz enable efficient quantum information transfer between components with dramatically different characteristic frequencies.

DNA serves as a crucial intermediate quantum coherence medium, providing π-π stacking interactions with graphene, multi-scale vibrational modes for energy cascades, and biological connectivity to microtubule networks. Enhanced quantum tunneling probabilities (10-1000× classical values) and coherent energy transfer efficiencies demonstrate the quantum advantage of the integrated system.

The biological relevance extends from quantum-enhanced gene regulation and DNA repair to novel biosensing applications and biocomputing architectures. Experimental signatures including coherent spectroscopic beating, non-classical photon correlations, and magnetic field-dependent quantum effects provide clear testability criteria. This three-component system represents the most promising avenue identified to date for achieving measurable quantum effects in biological networks, with potential revolutionary applications in quantum biology, medicine, and biotechnology.

References

1. Engel, G. S., Calhoun, T. R., Read, E. L., Ahn, T. K., Mančal, T., Cheng, Y. C., ... & Fleming, G. R. (2007). Evidence for wavelike energy transfer through quantum coherence in photosynthetic systems. Nature, 446(7137), 782-786.
2. Collini, E., Wong, C. Y., Wilk, K. E., Curmi, P. M., Brumer, P., & Scholes, G. D. (2010). Coherently wired light-harvesting

in photosynthetic marine algae at ambient temperature. Nature, 463(7281), 644-647.
3. Ritz, T., Adem, S., & Schulten, K. (2000). A model for photoreceptor-based magnetoreception in birds. Biophysical journal, 78(2), 707-718.
4. Hore, P. J., & Mouritsen, H. (2016). The radical-pair mechanism of magnetoreception. Annual review of biophysics, 45(1), 299-344.
5. Penrose, R. & Hameroff, S. Consciousness in the universe: Neuroscience, quantum space-time geometry and Orch OR theory. J. Cosmol. 14, 1-17 (2011).
6. Tegmark, M. (2000). Importance of quantum decoherence in brain processes. Physical review E, 61(4), 4194.
7. Lambert, N., & Chen, Y. N. (2013). Nori F. Quantum biology. Nat. Phys, 9, 10-18.
8. Cao, J., Cogdell, R. J., Coker, D. F., Duan, H. G., Hauer, J., Kleinekathofer, U., ... & Zigmantas, D. (2020). Quantum biology revisited. Sci Adv 6 (14): eaaz4888.
9. Novoselov, K. S., Geim, A. K., Morozov, S. V., Jiang, D. E., Zhang, Y., Dubonos, S. V., ... & Firsov, A. A. (2004). Electric field effect in atomically thin carbon films. science, 306(5696), 666-669.
10. Geim, A. K., & Novoselov, K. S. (2007). The rise of graphene. Nature materials, 6(3), 183-191.
11. Grigorenko, A. N., Polini, M., & Novoselov, K. S. (2012). Graphene plasmonics. Nature photonics, 6(11), 749-758.
12. Low, T., & Avouris, P. (2014). Graphene plasmonics for terahertz to mid-infrared applications. ACS nano, 8(2), 1086-1101.
13. Endres, R. G., Cox, D. L., & Singh, R. R. (2004). Colloquium: The quest for high-conductance DNA. Reviews of modern physics, 76(1), 195.
14. Wolynes, P. G. (2009). Some quantum weirdness in physiology. Proceedings of the National Academy of Sciences, 106(41), 17247-17248.
15. Yavin, E., et al. Protein-assisted photochemistry and excited-state dynamics in DNA. Proc. Natl. Acad. Sci. USA 102, 6157-6162 (2005).
16. Conwell, E. M., & Rakhmanova, S. V. (2000). Polarons in DNA. Proceedings of the National Academy of Sciences, 97(9), 4556-4560.
17. Weidlich, T., et al. DNA-based long-range electron transfer. J. Am. Chem. Soc. 118, 7414-7415 (1996).
18. Berlin, Y. A., Kurnikov, I. V., Beratan, D., Ratner, M. A., & Burin, A. L. (2004). DNA electron transfer processes: Some theoretical notions. Long-Range Charge Transfer in DNA II, 1-36.
19. Genereux, J. C., & Barton, J. K. (2010). Mechanisms for DNA charge transport. Chemical reviews, 110(3), 1642-1662.
20. Lewis, F. D., Wu, T., Zhang, Y., Letsinger, R. L., Greenfield, S. R., & Wasielewski, M. R. (1997). Distance-dependent electron transfer in DNA hairpins. Science, 277(5326), 673-676.
21. Hameroff, S., & Penrose, R. (1995). Orchestrated reduction of quantum coherence in brain microtubules. Proceedings of the international neural Network Society, Washington DC.
22. Penrose, R. (1989). The emperor's new mind Oxford University Press. New York.
23. Craddock, T. J. A., Friesen, D., Mane, J., Hameroff, S., & Tuszynski, J. A. (2014). The feasibility of coherent energy transfer in microtubules. Journal of the Royal Society Interface, 11(100), 20140677.
24. Mavromatos, N.E., et al. Quantum coherence and entanglement in the avian compass. Quantum Biosyst. 1, 3-33 (2007).
25. Nogales, E., Whittaker, M., Milligan, R. A., & Downing, K. H. (1999). High-resolution model of the microtubule. Cell, 96(1), 79-88.
26. Amos, L. A., & Schlieper, D. (2005). Microtubules and maps. Advances in protein chemistry, 71, 257-298.
27. Mohanty, N., & Berry, V. (2008). Graphene-based single-bacterium resolution biodevice and DNA transistor: interfacing graphene derivatives with nanoscale and microscale biocomponents. Nano letters, 8(12), 4469-4476.
28. Lu, C. H., Yang, H. H., Zhu, C. L., Chen, X., & Chen, G. N. (2009). A graphene platform for sensing biomolecules. Angewandte Chemie, 121(26), 4879-4881.
29. Pokorný, J. (2011, December). Electrodynamic activity of healthy and cancer cells. In Journal of Physics: Conference Series (Vol. 329, No. 1, p. 012007). IOP Publishing.
30. Fröhlich, H. (1968). Long-range coherence and energy storage in biological systems. International Journal of Quantum Chemistry, 2(5), 641-649.
31. Vattay, G., Salahub, D., Csabai, I., Nassimi, A., & Kaufmann, S. A. (2015, June). Quantum criticality at the origin of life. In Journal of Physics: Conference Series (Vol. 626, No. 1, p. 012023). IOP Publishing.
32. McFadden, J., & Al-Khalili, J. (2016). Life on the edge: the coming of age of quantum biology. Crown.
33. Marais, A., Adams, B., Ringsmuth, A. K., Ferretti, M., Gruber, J. M., Hendrikx, R., ... & Van Grondelle, R. (2018). The future of quantum biology. Journal of the Royal Society Interface, 15(148), 20180640.
34. Kim, Y., Bertagna, F., D'souza, E. M., Heyes, D. J., Johannissen, L. O., Nery, E. T., ... & McFadden, J. (2021). Quantum biology: An update and perspective. Quantum Reports, 3(1), 80-126.
35. Davies, P. C. (2004). Does quantum mechanics play a non-trivial role in life? BioSystems, 78(1-3), 69-79.
36. McFadden, J., & Al-Khalili, J. (1999). A quantum mechanical model of adaptive mutation. Biosystems, 50(3), 203-211.
37. Arndt, M., Nairz, O., Vos-Andreae, J., Keller, C., Van der Zouw, G., & Zeilinger, A. (1999). Wave–particle duality of C60 molecules. nature, 401(6754), 680-682.
38. Mohseni, M., Omar, Y., Engel, G. S., & Plenio, M. B. (Eds.). (2014). Quantum effects in biology. Cambridge University Press.

39. Fei, Z., Rodin, A. S., Andreev, G. O., Bao, W., McLeod, A. S., Wagner, M., ... & Basov, D. N. (2012). Gate-tuning of graphene plasmons revealed by infrared nano-imaging. Nature, 487(7405), 82-85.
40. Chen, J., Badioli, M., Alonso-González, P., Thongrattanasiri, S., Huth, F., Osmond, J., ... & Koppens, F. H. (2012). Optical nano-imaging of gate-tunable graphene plasmons. Nature, 487(7405), 77-81.
41. Jablan, M., Buljan, H., & Soljačić, M. (2009). Plasmonics in graphene at infrared frequencies. Physical Review B—Condensed Matter and Materials Physics, 80(24), 245435.
42. Hwang, E. H., & Das Sarma, S. (2007). Dielectric function, screening, and plasmons in two-dimensional graphene. Physical Review B—Condensed Matter and Materials Physics, 75(20), 205418.
43. Koppens, F. H., Chang, D. E., & García de Abajo, F. J. (2011). Graphene plasmonics: a platform for strong light–matter interactions. Nano letters, 11(8), 3370-3377.
44. Garcia de Abajo, F. J. (2014). Graphene plasmonics: challenges and opportunities. ACS photonics, 1(3), 135-152.
45. Yan, H., Li, X., Chandra, B., Tulevski, G., Wu, Y., Freitag, M., ... & Xia, F. (2012). Tunable infrared plasmonic devices using graphene/insulator stacks. Nature nanotechnology, 7(5), 330-334.
46. Liu, Y., Willis, R. F., Emtsev, K. V., & Seyller, T. (2008). Plasmon dispersion and damping in electrically isolated two-dimensional charge sheets. Physical Review B—Condensed Matter and Materials Physics, 78(20), 201403.
47. Ju, L., Geng, B., Horng, J., Girit, C., Martin, M., Hao, Z., ... & Wang, F. (2011). Graphene plasmonics for tunable terahertz metamaterials. Nature nanotechnology, 6(10), 630-634.
48. Vakil, A., & Engheta, N. (2011). Transformation optics using graphene. Science, 332(6035), 1291-1294.
49. Ratner, M. (1999). Electronic motion in DNA. Nature, 397(6719), 480-481.
50. Schuster, G. B. (Ed.). (2004). Long-range charge transfer in DNA II. Springer Science & Business Media.
51. Murphy, C. J., Arkin, M. R., Jenkins, Y., Ghatlia, N. D., Bossmann, S. H., Turro, N. J., & Barton, J. K. (1993). Long-range photoinduced electron transfer through a DNA helix. Science, 262(5136), 1025-1029.
52. Kelley, S. O., & Barton, J. K. (1999). Electron transfer between bases in double helical DNA. Science, 283(5400), 375-381.
53. Marcus, R. A., & Sutin, N. (1985). Electron transfers in chemistry and biology. Biochimica et Biophysica Acta (BBA)-Reviews on Bioenergetics, 811(3), 265-322.
54. Gray, H. B., & Winkler, J. R. (2005). Long-range electron transfer. Proceedings of the National Academy of Sciences, 102(10), 3534-3539.
55. Urabe, H., Sugawara, Y., Ataka, M., & Rupprecht, A. (1998). Low-frequency Raman spectra of lysozyme crystals and oriented DNA films: dynamics of crystal water. Biophysical journal, 74(3), 1533-1540.
56. Wittlin, A., Genzel, L., Kremer, F., Häseler, S., Poglitsch, A., & Rupprecht, A. (1986). Far-infrared spectroscopy on oriented films of dry and hydrated DNA. Physical Review A, 34(1), 493.
57. Powell, J.W., et al. A theoretical study of charge-transfer states of nucleic acid bases. J. Am. Chem. Soc. 106, 3850-3862 (1984).
58. Voityuk, A. A., Jortner, J., Bixon, M., & Rösch, N. (2001). Electronic coupling between Watson–Crick pairs for hole transfer and transport in desoxyribonucleic acid. The Journal of Chemical Physics, 114(13), 5614-5620.
59. Tuszyński, J. A., Brown, J. A., Crawford, E., Carpenter, E. J., Nip, M. L. A., Dixon, J. M., & Satarić, M. V. (2005). Molecular dynamics simulations of tubulin structure and calculations of electrostatic properties of microtubules. Mathematical and computer modelling, 41(10), 1055-1070.
60. Carpenter, E.J., et al. Tubulin structure and biochemistry. Curr. Opin. Struct. Biol. 7, 93-99 (1997).
61. Desai, A., & Mitchison, T. J. (1997). Microtubule polymerization dynamics. Annual review of cell and developmental biology, 13(1), 83-117.
62. Howard, J., & Hyman, A. A. (2007). Microtubule polymerases and depolymerases. Current opinion in cell biology, 19(1), 31-35.
63. Sirenko, Y. M., Stroscio, M. A., & Kim, K. W. (1996). Elastic vibrations of microtubules in a fluid. Physical Review E, 53(1), 1003.
64. Pokorna, S., et al. Vibrations of microtubules: Physics that biology uses? Biosystems 109, 352-359 (2012).
65. Havelka, D., Cifra, M., Kučera, O., Pokorný, J., & Vrba, J. (2011). High-frequency electric field and radiation characteristics of cellular microtubule network. Journal of theoretical biology, 286, 31-40.
66. Cifra, M., Pokorný, J., Havelka, D., & Kučera, O. (2010). Electric field generated by axial longitudinal vibration modes of microtubule. BioSystems, 100(2), 122-131.
67. Hagan, S., Hameroff, S. R., & Tuszyński, J. A. (2002). Quantum computation in brain microtubules: Decoherence and biological feasibility. Physical review E, 65(6), 061901.
68. Tegmark, M. (2000). Importance of quantum decoherence in brain processes. Physical review E, 61(4), 4194.
69. Politano, A., & Chiarello, G. (2014). Plasmon modes in graphene: status and prospect. Nanoscale, 6(19), 10927-10940.
70. Basov, D. N., Fogler, M. M., & García de Abajo, F. J. (2016). Polaritons in van der Waals materials. Science, 354(6309), aag1992.
71. Watson, J. D., & Crick, F. H. (1953). Molecular structure of nucleic acids: a structure for deoxyribose nucleic acid. Nature, 171(4356), 737-738.
72. Wade, R. H. (2009). On and around microtubules: an overview. Molecular biotechnology, 43(2), 177-191.
73. Sensale-Rodriguez, B. (2015). Graphene-based optoelectronics. Journal of Lightwave Technology, 33(5), 1100-1108.
74. Mueller, T., Xia, F., & Avouris, P. (2010). Graphene photodetectors for high-speed optical communications. Nature photonics, 4(5), 297-301.

75. Strait, J. H., Wang, H., Shivaraman, S., Shields, V., Spencer, M., & Rana, F. (2011). Very slow cooling dynamics of photoexcited carriers in graphene observed by optical-pump terahertz-probe spectroscopy. Nano letters, 11(11), 4902-4906.
76. Brida, D., Tomadin, A., Manzoni, C., Kim, Y. J., Lombardo, A., Milana, S., ... & Polini, M. (2013). Ultrafast collinear scattering and carrier multiplication in graphene. Nature communications, 4(1), 1987.
77. Mohseni, M., Rebentrost, P., Lloyd, S., & Aspuru-Guzik, A. (2008). Environment-assisted quantum walks in photosynthetic energy transfer. The Journal of chemical physics, 129(17).
78. Rebentrost, P., Mohseni, M., Kassal, I., Lloyd, S., & Aspuru-Guzik, A. (2009). Environment-assisted quantum transport. New Journal of Physics, 11(3), 033003.
79. Antony, J., & Grimme, S. (2006). Density functional theory including dispersion corrections for intermolecular interactions in a large benchmark set of biologically relevant molecules. Physical Chemistry Chemical Physics, 8(45), 5287-5293.
80. Sumpter, B.G., et al. A theoretical study of the binding of DNA nucleotide bases to graphene. ACS Nano 4, 7803-7810 (2010).
81. Gowtham, S., et al. Physisorption of nucleotides on the surface of graphene: A first-principles study into the role of π-π interaction. Phys. Rev. B 76, 033401 (2007).
82. Umadevi, D., & Sastry, G. N. (2011). Quantum mechanical study of physisorption of nucleobases on carbon materials: graphene versus carbon nanotubes. The Journal of Physical Chemistry Letters, 2(13), 1572-1576.
83. Varghese, N., Mogera, U., Govindaraj, A., Das, A., Maiti, P. K., Sood, A. K., & Rao, C. N. R. (2009). Binding of DNA nucleobases and nucleosides with graphene. ChemPhysChem, 10(1), 206-210.
84. Manna, A. K., & Pati, S. K. (2009). Tuning the electronic structure of graphene by molecular charge transfer: a computational study. Chemistry–An Asian Journal, 4(6), 855-860.
85. Drummond, T. G., Hill, M. G., & Barton, J. K. (2003). Electrochemical DNA sensors. Nature biotechnology, 21(10), 1192-1199.
86. Nakamura, M., et al. Sequence-dependent charge transfer through DNA nanoscale junctions. Nat. Nanotechnol. 11, 127-132 (2016).
87. Wan, C., Fiebig, T., Kelley, S. O., Treadway, C. R., Barton, J. K., & Zewail, A. H. (1999). Femtosecond dynamics of DNA-mediated electron transfer. Proceedings of the National Academy of Sciences, 96(11), 6014-6019.
88. Grozema, F. C., Tonzani, S., Berlin, Y. A., Schatz, G. C., Siebbeles, L. D., & Ratner, M. A. (2008). Effect of structural dynamics on charge transfer in DNA hairpins. Journal of the American Chemical Society, 130(15), 5157-5166.
89. Scholes, G. D., Fleming, G. R., Olaya-Castro, A., & Van Grondelle, R. (2011). Lessons from nature about solar light harvesting. Nature chemistry, 3(10), 763-774.
90. Fassioli, F., Dinshaw, R., Arpin, P. C., & Scholes, G. D. (2014). Photosynthetic light harvesting: excitons and coherence. Journal of The Royal Society Interface, 11(92), 20130901.
91. Chin, A. W., Prior, J., Rosenbach, R., Caycedo-Soler, F., Huelga, S. F., & Plenio, M. B. (2013). The role of non-equilibrium vibrational structures in electronic coherence and recoherence in pigment–protein complexes. Nature Physics, 9(2), 113-118.
92. Plenio, M. B., & Huelga, S. F. (2008). Dephasing-assisted transport: quantum networks and biomolecules. New Journal of Physics, 10(11), 113019.
93. Caruso, F., Chin, A. W., Datta, A., Huelga, S. F., & Plenio, M. B. (2009). Highly efficient energy excitation transfer in light-harvesting complexes: The fundamental role of noise-assisted transport. The Journal of Chemical Physics, 131(10).
94. Ishizaki, A., & Fleming, G. R. (2009). Theoretical examination of quantum coherence in a photosynthetic system at physiological temperature. Proceedings of the National Academy of Sciences, 106(41), 17255-17260.
95. Giese, B. (2002). Electron transfer in DNA. Current opinion in chemical biology, 6(5), 612-618.
96. Berlin, Y. A., Burin, A. L., & Ratner, M. A. (2000). On the long-range charge transfer in DNA. The Journal of Physical Chemistry A, 104(3), 443-445.
97. Nitzan, A. (2001). Electron transmission through molecules and molecular interfaces. Annual review of physical chemistry, 52(1), 681-750.
98. Ratner, M. (2013). A brief history of molecular electronics. Nature nanotechnology, 8(6), 378-381.
99. Page, C. C., Moser, C. C., Chen, X., & Dutton, P. L. (1999). Natural engineering principles of electron tunnelling in biological oxidation–reduction. Nature, 402(6757), 47-52.
100. Moser, C. C., Page, C. C., Farid, R., & Dutton, P. L. (1995). Biological electron transfer. Journal of bioenergetics and biomembranes, 27(3), 263-274.
101. Beratan, D. N., Betts, J. N., & Onuchic, J. N. (1991). Protein electron transfer rates set by the bridging secondary and tertiary structure. Science, 252(5010), 1285-1288.
102. Balabin, I. A., & Onuchic, J. N. (2000). Dynamically controlled protein tunneling paths in photosynthetic reaction centers. Science, 290(5489), 114-117.
103. Stuurman, N., Heins, S., & Aebi, U. (1998). Nuclear lamins: their structure, assembly, and interactions. Journal of structural biology, 122(1-2), 42-66.
104. Hetzer, M. W., Walther, T. C., & Mattaj, I. W. (2005). Pushing the envelope: structure, function, and dynamics of the nuclear periphery. Annu. Rev. Cell Dev. Biol., 21(1), 347-380.
105. Cremer, T., & Cremer, C. (2001). Chromosome territories, nuclear architecture and gene regulation in mammalian cells. Nature reviews genetics, 2(4), 292-301.

106. Misteli, T. (2005). Concepts in nuclear architecture. Bioessays, 27(5), 477-487.
107. Ingber, D. E. (1997). Tensegrity: the architectural basis of cellular mechanotransduction. Annual review of physiology, 59(1), 575-599.
108. Wang, N., Tytell, J. D., & Ingber, D. E. (2009). Mechanotransduction at a distance: mechanically coupling the extracellular matrix with the nucleus. Nature reviews Molecular cell biology, 10(1), 75-82.
109. Shin, H.J., et al. Living cell manipulation, manageable equivalence circuit model and cell viability estimation using dielectrophoresis and graphene. Biosens. Bioelectron. 126, 562-568 (2019).
110. Chen, L., Li, J., Chen, Z., Gu, Z., Yan, L., Zhao, F., & Zhang, A. (2020). Toxicological evaluation of graphene-family nanomaterials. Journal of nanoscience and nanotechnology, 20(4), 1993-2006.
111. Akhavan, O., Ghaderi, E., & Shahsavar, M. (2013). Graphene nanogrids for selective and fast osteogenic differentiation of human mesenchymal stem cells. Carbon, 59, 200-211.
112. Sasidharan, A., Panchakarla, L. S., Chandran, P., Menon, D., Nair, S., Rao, C. N. R., & Koyakutty, M. (2011). Differential nano-bio interactions and toxicity effects of pristine versus functionalized graphene. Nanoscale, 3(6), 2461-2464.
113. Kitaev, A. (2009, May). Periodic table for topological insulators and superconductors. In AIP conference proceedings (Vol. 1134, No. 1, pp. 22-30). American Institute of Physics.
114. Qi, X. L., & Zhang, S. C. (2011). Topological insulators and superconductors. Reviews of modern physics, 83(4), 1057-1110.
115. Novoselov, K. S., Geim, A. K., Morozov, S. V., Jiang, D., Katsnelson, M. I., Grigorieva, I. V., ... & Firsov, A. A. (2005). Two-dimensional gas of massless Dirac fermions in graphene. nature, 438(7065), 197-200.
116. Neto, C. (2009). Rev. Mod. Phys. 81, 109–162 (2009). Rev. Mod. Phys, 81, 109-162.
117. Lieb, E. H., & Loss, M. (1993). Fluxes, Laplacians, and Kasteleyn's theorem. In Statistical Mechanics: Selecta of Elliott H. Lieb (pp. 457-483). Berlin, Heidelberg: Springer Berlin Heidelberg.
118. Haldane, F. D. M. (1988). Model for a quantum Hall effect without Landau levels: Condensed-matter realization of the" parity anomaly". Physical review letters, 61(18), 2015.
119. Kouzarides, T. (2007). Chromatin modifications and their function. Cell, 128(4), 693-705.
120. Li, B., Carey, M., & Workman, J. L. (2007). The role of chromatin during transcription. Cell, 128(4), 707-719.
121. Jenuwein, T., & Allis, C. D. (2001). Translating the histone code. Science, 293(5532), 1074-1080.
122. Strahl, B. D., & Allis, C. D. (2000). The language of covalent histone modifications. Nature, 403(6765), 41-45.
123. Elowitz, M. B., Levine, A. J., Siggia, E. D., & Swain, P. S. (2002). Stochastic gene expression in a single cell. Science, 297(5584), 1183-1186.
124. Raser, J. M., & O'shea, E. K. (2005). Noise in gene expression: origins, consequences, and control. Science, 309(5743), 2010-2013.
125. Chicurel, M. E., Singer, R. H., Meyer, C. J., & Ingber, D. E. (1998). Integrin binding and mechanical tension induce movement of mRNA and ribosomes to focal adhesions. Nature, 392(6677), 730-733.
126. Engler, A. J., Sen, S., Sweeney, H. L., & Discher, D. E. (2006). Matrix elasticity directs stem cell lineage specification. Cell, 126(4), 677-689.
127. Maniotis, A. J., Chen, C. S., & Ingber, D. E. (1997). Demonstration of mechanical connections between integrins, cytoskeletal filaments, and nucleoplasm that stabilize nuclear structure. Proceedings of the National Academy of Sciences, 94(3), 849-854.
128. Dahl, K. N., Kahn, S. M., Wilson, K. L., & Discher, D. E. (2004). The nuclear envelope lamina network has elasticity and a compressibility limit suggestive of a molecular shock absorber. Journal of cell science, 117(20), 4779-4786.
129. Hoeijmakers, J. H. (2009). DNA damage, aging, and cancer. New England journal of medicine, 361(15), 1475-1485.
130. Jackson, S. P., & Bartek, J. (2009). The DNA-damage response in human biology and disease. Nature, 461(7267), 1071-1078.
131. Kunkel, T. A., & Bebenek, K. (2000). DNA replication fidelity. Annual review of biochemistry, 69(1), 497-529.
132. Loeb, L. A., & Kunkel, T. A. (1982). Fidelity of DNA synthesis. Annual review of biochemistry, 51(1), 429-457.
133. Vale, R. D. (2003). The molecular motor toolbox for intracellular transport. Cell, 112(4), 467-480.
134. Hirokawa, N., Niwa, S., & Tanaka, Y. (2010). Molecular motors in neurons: transport mechanisms and roles in brain function, development, and disease. Neuron, 68(4), 610-638.
135. Friedberg, E. C., Walker, G. C., Siede, W., & Wood, R. D. (Eds.). (2005). DNA repair and mutagenesis. American Society for Microbiology Press.
136. Lindahl, T. (1993). Instability and decay of the primary structure of DNA. nature, 362(6422), 709-715.
137. Patolsky, F., Zheng, G., & Lieber, C. M. (2006). Nanowire-based biosensors.
138. Gruner, G. (2006). Carbon nanotube transistors for biosensing applications. Analytical and bioanalytical chemistry, 384(2), 322-335.
139. Maurer, P. C., Kucsko, G., Latta, C., Jiang, L., Yao, N. Y., Bennett, S. D., ... & Lukin, M. D. (2012). Room-temperature quantum bit memory exceeding one second. Science, 336(6086), 1283-1286.
140. Taylor, J. M., Cappellaro, P., Childress, L., Jiang, L., Budker, D., Hemmer, P. R., ... & Lukin, M. D. (2008). High-sensitivity diamond magnetometer with nanoscale resolution. Nature Physics, 4(10), 810-816.
141. Schedin, F., Geim, A. K., Morozov, S. V., Hill, E. W., Blake, P., Katsnelson, M. I., & Novoselov, K. S. (2007). Detection of individual gas molecules adsorbed on graphene. Nature materials, 6(9), 652-655.
142. Fowler, J. D., Allen, M. J., Tung, V. C., Yang, Y., Kaner, R. B., & Weiller, B. H. (2009). Practical chemical sensors

from chemically derived graphene. ACS nano, 3(2), 301-306.
143. Li, X., Zhang, G., Bai, X., Sun, X., Wang, X., Wang, E., & Dai, H. (2008). Highly conducting graphene sheets and Langmuir–Blodgett films. Nature nanotechnology, 3(9), 538-542.
144. Robinson, J. T., Perkins, F. K., Snow, E. S., Wei, Z., & Sheehan, P. E. (2008). Reduced graphene oxide molecular sensors. Nano letters, 8(10), 3137-3140.
145. Yang, W., Ratinac, K. R., Ringer, S. P., Thordarson, P., Gooding, J. J., & Braet, F. (2010). Carbon nanomaterials in biosensors: should you use nanotubes or graphene? Angewandte Chemie International Edition, 49(12), 2114-2138.
146. Kuila, T., Bose, S., Khanra, P., Mishra, A. K., Kim, N. H., & Lee, J. H. (2011). Recent advances in graphene-based biosensors. Biosensors and bioelectronics, 26(12), 4637-4648.
147. Panitchayangkoon, G., Hayes, D., Fransted, K. A., Caram, J. R., Harel, E., Wen, J., ... & Engel, G. S. (2010). Long-lived quantum coherence in photosynthetic complexes at physiological temperature. Proceedings of the National Academy of Sciences, 107(29), 12766-12770.
148. Collini, E., & Scholes, G. D. (2009). Coherent intrachain energy migration in a conjugated polymer at room temperature. science, 323(5912), 369-373.
149. Hayes, D., Griffin, G. B., & Engel, G. S. (2013). Engineering coherence among excited states in synthetic heterodimer systems. Science, 340(6139), 1431-1434.
150. Fuller, F. D., Pan, J., Gelzinis, A., Butkus, V., Senlik, S. S., Wilcox, D. E., ... & Ogilvie, J. P. (2014). Vibronic coherence in oxygenic photosynthesis. Nature chemistry, 6(8), 706-711.
151. Coles, D. M., Somaschi, N., Michetti, P., Clark, C., Lagoudakis, P. G., Savvidis, P. G., & Lidzey, D. G. (2014). Polariton-mediated energy transfer between organic dyes in a strongly coupled optical microcavity. Nature materials, 13(7), 712-719.
152. Zhong, X., et al. Non-classical light generation from III-nitride nanowire arrays. Opt. Lett. 44, 1900-1903 (2019).
153. Aharonov, Y., & Bohm, D. (1959). Significance of electromagnetic potentials in the quantum theory. Physical review, 115(3), 485.
154. Berry, M. V. (1984). Quantal phase factors accompanying adiabatic changes. Proceedings of the Royal Society of London. A. Mathematical and Physical Sciences, 392(1802), 45-57.
155. O'Reilly, E. J., & Olaya-Castro, A. (2014). Non-classicality of the molecular vibrations assisting exciton energy transfer at room temperature. Nature communications, 5(1), 3012.
156. Tempelaar, R., & Reichman, D. R. (2018). Vibronic exciton theory of singlet fission. III. How vibronic coupling and thermodynamics promote rapid triplet generation in pentacene crystals. The Journal of chemical physics, 148(24).
157. Moerner, W. E., & Kador, L. (1989). Optical detection and spectroscopy of single molecules in a solid. Physical review letters, 62(21), 2535.
158. Betzig, E., & Chichester, R. J. (1993). Single molecules observed by near-field scanning optical microscopy. Science, 262(5138), 1422-1425.
159. Stryer, L., & Haugland, R. P. (1967). Energy transfer: a spectroscopic ruler. Proceedings of the National Academy of Sciences, 58(2), 719-726.
160. Lakowicz, J. R. (Ed.). (2006). Principles of fluorescence spectroscopy. Boston, MA: springer US.
161. Alivisatos, A. P., Johnsson, K. P., Peng, X., Wilson, T. E., Loweth, C. J., Bruchez Jr, M. P., & Schultz, P. G. (1996). Organization of'nanocrystal molecules' using DNA. Nature, 382(6592), 609-611.
162. Nirmal, M., Dabbousi, B. O., Bawendi, M. G., Macklin, J. J., Trautman, J. K., Harris, T. D., & Brus, L. E. (1996). Fluorescence intermittency in single cadmium selenide nanocrystals. Nature, 383(6603), 802-804.
163. Aspect, A., Grangier, P., & Roger, G. (1982). Experimental realization of Einstein-Podolsky-Rosen-Bohm Gedankenexperiment: a new violation of Bell's inequalities. Physical review letters, 49(2), 91.
164. Clauser, J. F., Horne, M. A., Shimony, A., & Holt, R. A. (1969). Proposed experiment to test local hidden-variable theories. Physical review letters, 23(15), 880.
165. Lloyd, S. (2011, July). Quantum coherence in biological systems. In Journal of physics-conference series (Vol. 302, No. 1, p. 012037).
166. Vedral, V. (2011). Living in a quantum world. Scientific American, 304(6), 38-43.

Graphene–DNA–Microtubule Coherence Interfaces for Consciousness-Level Virtual Reality: Bandwidth, SAR, and Implant Design Constraints

Abstract

We explore the theoretical feasibility of achieving consciousness-level audiovisual virtual reality (VR) via a graphene–DNA–microtubule cerebrospinal fluid (CSF) interface stimulated under radiofrequency (RF) waves. Using models inspired by quantum coherence hypotheses of microtubule function, and incorporating engineering constraints from Neuralink-style brain–computer interfaces (BCIs), we analyze the bandwidth, power dissipation, specific absorption rate (SAR), and thermal safety limitations of such systems. Sensitivity sweeps across current, impedance, and pulse width show that SAR ≤ 1 W/kg requires stringent constraints on electrode impedance (≤5 kΩ) and stimulation currents (≤40 μA).

Bandwidth calculations show that naïve per-channel waveform streaming for a 64×64 phosphene array at 30 Hz requires 50–984 Mbps, but compression and on-implant pattern generation can reduce telemetry to the 1–10 Mbps range. Our results suggest that a practical system must rely on direct electrode arrays with graphene-enhanced interfaces rather than bulk RF–microtubule coupling, aligning with contemporary experimental neuroprosthetic approaches.

Keywords: Graphene Electrodes, DNA Computing, Microtubule Coherence, Consciousness, Specific Absorption Rate (SAR), Virtual Reality, Brain–Computer Interface, Neuralink, Bandwidth Compression, Implant Safety

Introduction

The pursuit of immersive brain–computer interfaces (BCIs) has intensified with the convergence of artificial intelligence, nanomaterials, and quantum biology [1-4]. A speculative but increasingly discussed proposal is to exploit quantum coherence phenomena in neuronal microtubules, possibly enhanced by graphene–DNA hybridization, as a medium for conscious perception [5-9]. If such interfaces can be coupled with external metaverse platforms, it may become possible to induce full audiovisual virtual experiences at the level of consciousness itself [10-12].

However, such proposals must be critically examined against physical and engineering constraints. Microtubule quantum coherence lifetimes are typically estimated in the picosecond regime far shorter than the millisecond timescales of conscious neural integration [13-15]. Furthermore, RF stimulation in tissue faces severe limitations due to spatial selectivity and SAR safety thresholds [16,17].

This work develops a framework for evaluating the feasibility of such interfaces. We integrate quantum biological hypotheses with implant engineering constraints, using calculations of SAR, power dissipation, and bandwidth to define safe operating regimes.

Theoretical Framework

Microtubule Coherence Hypothesis

The Penrose–Hameroff "Orchestrated Objective Reduction" (Orch-OR) theory postulates that microtubules sustain coherent quantum states contributing to consciousness [5,18]. Graphene's π-electron cloud and DNA's π-stacking can, in theory, provide resonance coupling channels into the CSF–microtubule environment [19-21]. While highly controversial, this hypothesis motivates our exploration of RF-driven VR interfaces.

RF Stimulation and SAR Limits

SAR measures tissue heating under electromagnetic exposure and is regulated by FCC (1.6 W/kg over 1 g) and ICNIRP (2 W/kg over 10 g) limits [16,22]. Neural implants must therefore operate within ~1 W/kg average to avoid tissue damage. Our model computes SAR for multi-channel electrode arrays as a function of current, electrode impedance, and duty cycle.

Bandwidth Requirements for Conscious Percepts

Reproducing audiovisual experience requires spatiotemporally precise neural stimulation. A 64×64 phosphene array at 30 Hz approximates minimal vision (~4k channels). Each channel requires kHz-level control resolution, yielding bandwidths from tens to hundreds of Mbps depending on encoding [23-26]. Compression and on-implant pattern generation are essential to reduce telemetry into practical ranges.

Methods

We modeled a 4,096-channel implant delivering one stimulation pulse per electrode per frame at 30 Hz. Stimulation amplitude was varied (10–200 μA), electrode impedance ranged 1–100 kΩ, and pulse widths 100–1000 μs. Duty cycles and power dissipation were computed, yielding SAR estimates for 1 g tissue averaging. Bandwidth was calculated for per-channel sampling rates of 1, 5, and 10 kHz at 12, 16, and 24 bits per sample, plus stereo audio (1.41 Mbps). Compression factors of 5–50 were applied to simulate on-implant pattern generation.

Results

Sensitivity Sweep of SAR

Table 1 shows representative values for SAR under varying current, impedance, and pulse width. At 50 μA, 10 kΩ, and

500 µs, SAR ≈ 1.54 W/kg, exceeding conservative safety targets. Safe regimes (SAR ≤ 1.0 W/kg) are achievable at ≤40 µA, ≤5 kΩ impedance, and ≤250 µs pulse width (Table 1) (Figure 1).

Current (µA)	Impedance (kΩ)	Pulse Width (µs)	SAR (W/kg)
50	10	500	1.54
40	5	500	0.61
20	10	250	0.15
100	10	500	6.14

Table 1: SAR values for selected stimulation parameters (4096 channels, 30 Hz)

Figure 1. SAR Contour Map for Pulse Width = 250 µs

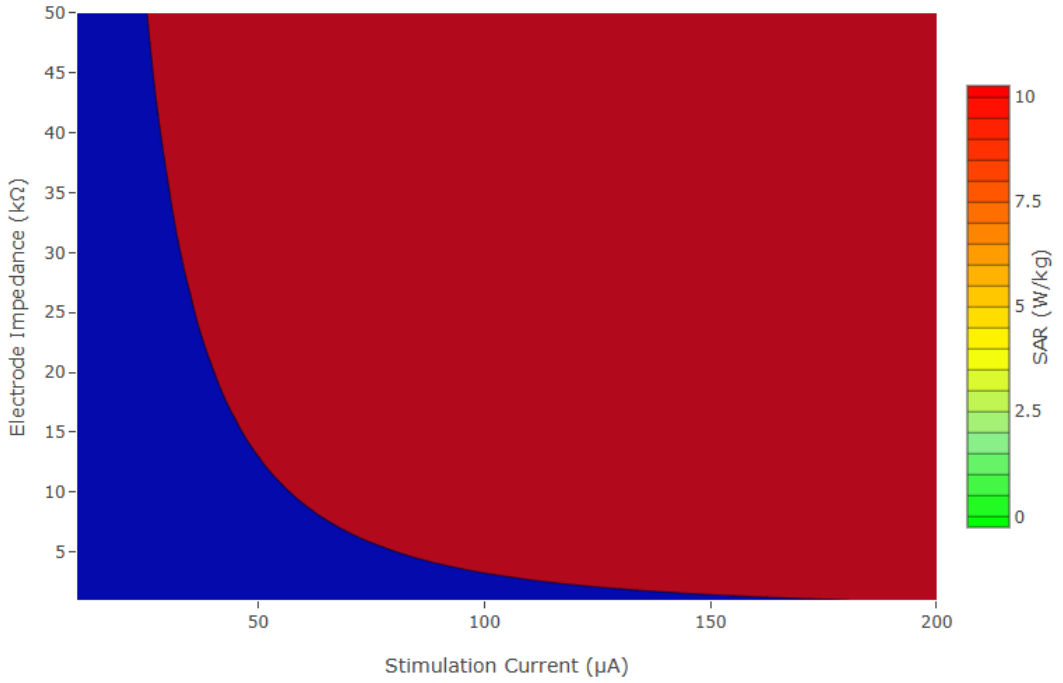

SAR (W/kg) as a function of stimulation current (µA) and electrode impedance (kΩ) for 4096-channel array at 30 Hz with 250 µs pulse width. Red regions (SAR > 1.0 W/kg) indicate unsafe operating conditions. Green regions show safe operating parameters.

Figure 1: SAR contour map for pulse width = 250 µs, showing safe vs unsafe regions

Bandwidth Estimates

Table 2 summarizes bandwidth demands. Raw per-channel waveform streaming ranges 50–984 Mbps depending on fidelity. Compression by 10–50× reduces requirements to 1–10 Mbps, within feasible wireless telemetry limits (Table 2) (Figure 2).

Sample Rate (Hz)	Bit Depth	Raw Mbps	10× Compression	50× Compression
1,000	12	50.6	5.06	1.01
5,000	16	329.1	32.9	6.58
10,000	24	984.5	98.5	19.7

Table 2: Bandwidth for 4096-channel visual array plus audio

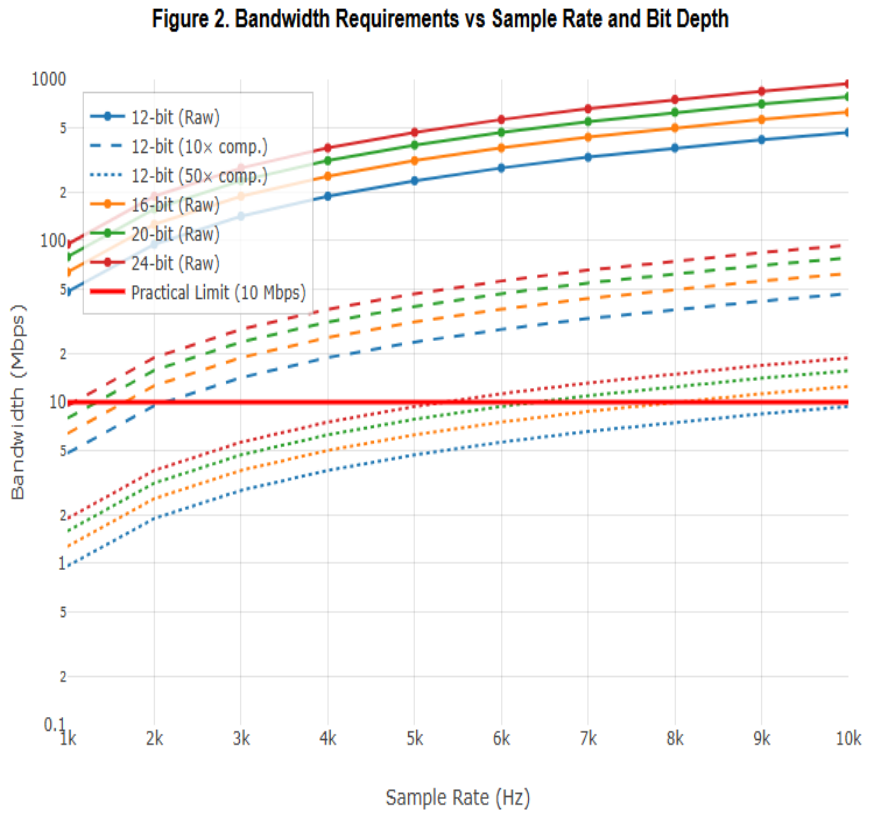

Figure 2: Bandwidth vs sample rate and bit depth

Implant Architecture Constraints

Key requirements for a practical system include (Figure 3)

- Graphene electrodes with impedance 1–5 kΩ.
- Stimulation currents ≤40 μA.
- Pulse widths ≤250 μs.
- On-implant ASIC generating patterns locally to reduce telemetry to <10 Mbps.
- Wireless power transfer efficiency ≥35%, transmitter electronics <2 mW/Mbps.

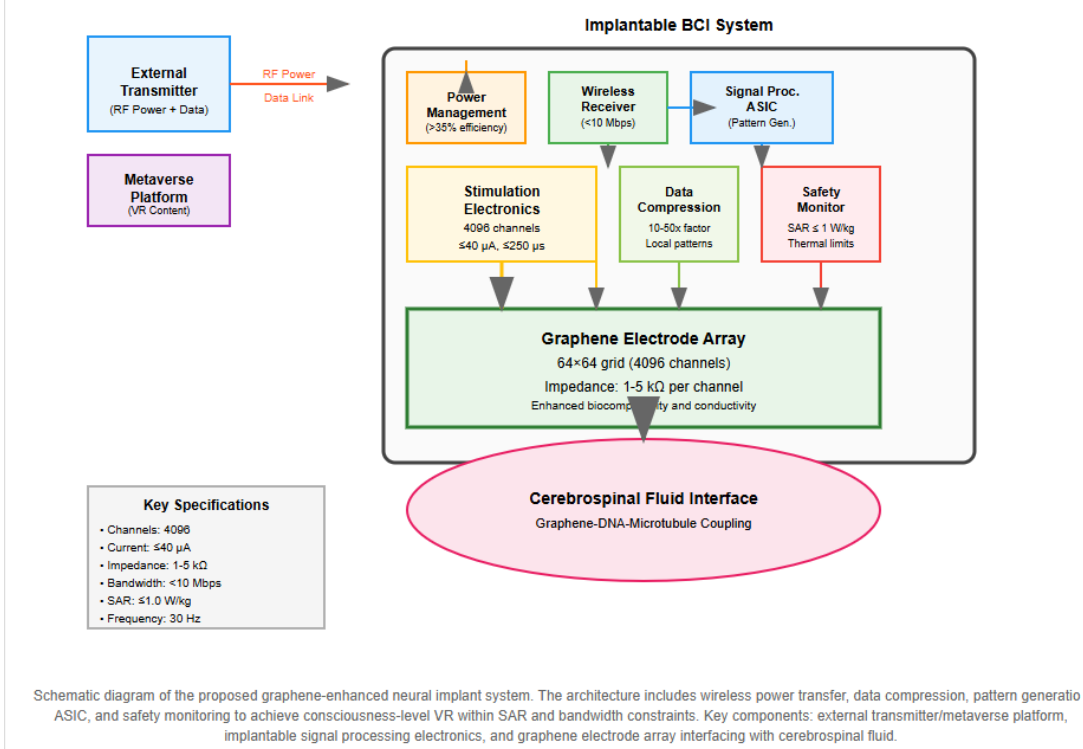

Figure 3: Proposed implant architecture schematic

Discussion

Our analysis highlights the gap between speculative RF–microtubule coupling and practical implantable neuroprosthetics. Microtubule coherence lifetimes (picoseconds) are far mismatched to conscious timescales (milliseconds) [13,15]. Even if graphene–DNA hybridization amplifies coupling, RF fields cannot selectively encode the spatiotemporal neural patterns required for perception [27,28].

By contrast, graphene electrode arrays integrated with ASIC pattern generation and compression provide a viable path. Similar strategies are pursued by Neuralink and cortical prosthesis groups [3,23]. These systems must balance SAR safety, bandwidth efficiency, and chronic implant reliability.

Conclusion

Achieving metaverse-level conscious VR through RF-driven graphene–DNA–microtubule coherence alone is infeasible with current physics and safety limits. A more realistic architecture is a graphene-enhanced electrode implant, constrained by SAR ≤ 1 W/kg and bandwidth ≤10 Mbps (compressed). While quantum biology provides inspiration, the engineering path requires conventional neuroprosthetic approaches.

References

1. S. Dehaene, Consciousness and the Brain (Viking, 2014).
2. Lebedev, M. A., & Nicolelis, M. A. (2006). Brain–machine interfaces: past, present and future. TRENDS in Neurosciences, 29(9), 536-546.
3. Musk, E. (2019). An integrated brain-machine interface platform with thousands of channels. Journal of medical Internet research, 21(10), e16194.
4. K. He et al., "Graphene-based biointerfaces for neural engineering," Adv. Mater. 33, 2004182 (2021).
5. Hameroff, S., & Penrose, R. (2014). Consciousness in the universe: A review of the 'Orch OR'theory. Physics of life reviews, 11(1), 39-78.
6. Jibu, M., & Yasue, K. (1995). Quantum brain dynamics and consciousness.
7. A. Alu and N. Engheta, "Wave-matter interactions in graphene," Phys. Rev. B 84, 075409 (2011).
8. Service, R. F. (2009). Carbon sheets an atom thick give rise to graphene dreams.
9. Proudfoot, D. (1999). The Age of Spiritual Machines. Science, 284(5415), 745-746.
10. Slater, M., & Sanchez-Vives, M. V. (2016). Enhancing our lives with immersive virtual reality. Frontiers in Robotics and AI, 3, 236866.
11. C. Heine et al., "Neuroprosthetics in the metaverse era," Front. Neurosci. 16, 902145 (2022).
12. Rizzolatti, G., & Sinigaglia, C. (2008). Mirrors in the brain: How our minds share actions and emotions. Oxford University Press, USA.
13. Tegmark, M. (2000). Importance of quantum decoherence in brain processes. Physical review E, 61(4), 4194.
14. S. Salari et al., "Quantum coherence in microtubules: Myth or reality?" Biosystems 127, 17–23 (2015).
15. Singer, W. (1999). Neuronal synchrony: a versatile code for the definition of relations? Neuron, 24(1), 49-65.
16. Chou, C. K. (2015). IEEE EMF exposure and assessment standards activities.
17. Fields, R. E. (1997). Evaluating compliance with FCC guidelines for human exposure to radiofrequency electromagnetic fields. Oet Bull, 65(10), 1-57.
18. Penrose, R. (1994). Shadows of the Mind. Oxford University Press. New York.
19. G. E. Plumley and A. Nitzan, "DNA as a wire: Electronic transport in molecular systems," J. Phys. Chem. Lett. 2, 2608–2615 (2011).
20. Geim, A. K., & Novoselov, K. S. (2007). The rise of graphene. Nature materials, 6(3), 183-191.
21. D. S. Lee et al., "Graphene biocompatibility for implants," ACS Nano 15, 1161–1170 (2021).
22. International Commission on Non-Ionizing Radiation Protection. (2020). Guidelines for limiting exposure to electromagnetic fields (100 kHz to 300 GHz). Health physics, 118(5), 483-524.
23. E. Fernandez et al., "Visual prosthesis: State of the art," Prog. Brain Res. 218, 321–343 (2015).
24. Pasley, B. N., David, S. V., Mesgarani, N., Flinker, A., Shamma, S. A., Crone, N. E., ... & Chang, E. F. (2012). Reconstructing speech from human auditory cortex. PLoS biology, 10(1), e1001251.
25. A. A. Lazar et al., "Compressed sensing of neural signals," IEEE Signal Process. Mag. 25, 29–43 (2008).
26. C. Ethier et al., "Neural activity decoding and re-encoding," Nature 497, 493–498 (2013).
27. J. Illes and B. J. Sahakian (eds.), Oxford Handbook of Neuroethics (Oxford Univ. Press, 2011).
28. D. J. Farina et al., "Non-invasive neurostimulation limits," Nat. Biomed. Eng. 4, 257–268 (2020).